NOLTR 66-54

LAMINAR AND TURBULENT BOUNDARY LAYERS ON SLIGHTLY-BLUNTED CONES AT HYPERSONIC SPEEDS

Code 1

21 MARCH 1966

NOL

UNITED STATES NAVAL ORDNANCE LABORATORY, WHITE OAK, MARYLAND

NOLTR 66-54

NOLTR 66-54

LAMINAR AND TURBULENT BOUNDARY LAYERS ON SLIGHTLY-BLUNTED CONES AT HYPERSONIC SPEEDS

21 MARCH 1966

NOL

UNITED STATES NAVAL ORDNANCE LABORATORY, WHITE OAK, MARYLAND

NOLTR 66-54

LAMINAR AND TURBULENT BOUNDARY LAYERS ON SLIGHTLY-BLUNTED CONES AT HYPERSONIC SPEEDS

Prepared by:

R. E. Wilson

ABSTRACT: A momentum-integral method for calculating the boundary-layer growth on slightly-blunted cones has been given in a previous paper by the writer. The method, which was applied to cones with fully laminar flow, is extended in the present paper to turbulent flow. In addition: (1) transition data on cones at hypersonic speeds are examined to show the great effect of slight nose blunting on interpretation of the results, (2) agreement between measured and calculated cone drag coefficients for fully laminar flow is demonstrated, and (3) turbulent friction and boundary-layer thickness calculations are shown to agree with the limited amount of ballistics range data which are available.

U. S. NAVAL ORDNANCE LABORATORY
White Oak, Silver Spring, Maryland

NOLTR 66-54 21 March 1966

LAMINAR AND TURBULENT BOUNDARY LAYERS ON SLIGHTLY-BLUNTED CONES AT HYPERSONIC SPEEDS

This report was presented as a paper at the AGARD Specialists' Meeting on "Recent Developments in Boundary Layer Research," sponsored by the Fluid Dynamics Panel of AGARD, Naples, 10-14 May 1965 and published in AGARDograph 97. Several changes have since been made.

The author would like to acknowledge the great amount of help received from Messrs. W. Carson Lyons, Jr. and Hensel Brown of the Ballistics Department. Mr. Lyons provided much of the experimental data shown here and Mr. Brown wrote a computer program and provided the numerical results.

J. A. DARE
Commander
Captain, USN

R. E. Wilson

R. E. WILSON
By direction

CONTENTS

ILLUSTRATIONS

List of Symbols

a = shock radius of curvature

b = tip radius of curvature

B = base radius

C_{D_o} = drag coefficient at zero angle of attack

$c_f = 2\tau_w/\rho_1 u_1^2$ = local skin friction coefficient

$c_{f_c} = 2\tau_w/\rho_c u_c^2$

F_1 = function defined by Eq. (19)

$H = \delta^*/\theta$ = boundary-layer shape parameter

L = body length

M = Mach number

P = pressure

Pr = Prandtl number

r = local cone radius

r_s = radius of streamtube in undisturbed flow

T = temperature

x = distance along cone surface measured from apex

y = distance normal to surface

γ = ratio of specific heats

δ = boundary-layer thickness

$\delta^* = \int_0^\delta [1 - (\rho u/\rho_1 u_1)]\, dy$ = boundary-layer displacement thickness

θ = $\int_0^{\delta} (\rho u/\rho_1 u_1)[1 - (u/u_1)]\,dy$ = boundary-layer momentum thickness

μ = absolute viscosity

R = Reynolds number: $R_{xc} = \rho_c u_c x/\mu_c$; $R_{\theta c} = \rho_c u_c \theta/\mu_c$;

$R_{bc} = \rho_c u_c b/\mu_c$; $R_{\theta 1} = \rho_1 u_1 \theta/\mu_1$; $R_{L\infty} = \rho_\infty u_\infty L/\mu_\infty$

ρ = density

σ = cone half angle

τ = shear stress

ω = shock wave angle for sharp cone

ω_s = local shock wave angle for blunt cone

Subscripts

c = conditions at the outer edge of the boundary layer on a sharp cone

w = conditions at the wall

1 = local conditions at the outer edge of the boundary layer

∞ = freestream conditions

T = stagnation conditions

Superscripts

o = sharp cone values

LAMINAR AND TURBULENT BOUNDARY LAYERS ON SLIGHTLY-BLUNTED CONES AT HYPERSONIC SPEEDS

INTRODUCTION

The momentum-integral method presented in reference (1) yields local flow conditions over slightly-blunted cones and at the same time yields values for the boundary-layer thicknesses, δ, δ^*, and θ. In addition, shear stress and heat-transfer distributions over the cone are determined. Reference (1) gives a skin-friction relation and expressions for the boundary-layer thicknesses which apply only to laminar flow. In the present paper relations are given for turbulent boundary-layer flow so that the solution of the momentum-integral equation can be continued after transition.

For the laminar boundary-layer case, references (2) and (3) give a method for calculating the local Mach number variation along the cone which assumes local similarity and makes use of a mass flow function of reference (4). The method does not account for the effect of Mach number gradient on boundary-layer growth. In addition, the method holds only for the case of highly-cooled walls. The momentum-integral method presented in reference (1) and used here does not have these limitations. A comparison was made in reference (1) between the momentum-integral method and the method of reference (2). There is a difference between references (2) and (3) which greatly affects numerical results and therefore both references have been compared here with the momentum-integral method.

The shear stress at the outer edge of the boundary layer is neglected in the momentum-integral equation. The accuracy in this assumption is commented on in reference (1). An expression for calculating the ratio, τ_1/τ_w for the laminar boundary layer is derived here so that this assumption can be checked for any specific case.

The ballistics ranges at the U. S. Naval Ordnance Laboratory have been used to measure transition on cones, the drag of fully laminar cones, the drag of cones with turbulent flow, and even to get some idea of the thickness of the turbulent boundary layer at the base of a cone. These data have been examined and pertinent calculations using the momentum-integral method have been made. The calculations have been compared

with experiment in some cases and in others have been used in analyzing the experimental data.

Theoretical Results

Momentum-Integral Equation

Using the coordinate system on figure 1, the momentum-integral equation for the conical part of a slightly-blunted cone is given in reference (1) as

$$\frac{d\theta}{dx} + \frac{2\theta}{M_1}\left\{1 - \frac{[(\delta/\theta) - H]}{2 + (\gamma-1)M_1^2}\right\}\frac{dM_1}{dx} + \frac{\theta}{r}\frac{dr}{dx} = c_f/2 \qquad (1)$$

The assumptions made in deriving equation (1) are: (1) a constant pressure on the conical surface equal to the inviscid sharp cone pressure, (2) a thermally and calorifically perfect gas, (3) adiabatic flow outside the boundary layer, and (4) $2\tau_1/\rho_1 u_1^2 \ll c_f$.

Boundary-Layer Parameters

The expressions for c_f, δ/θ, and H are taken from the flat plate case and evaluated at the local flow conditions at each point along the body. The expressions which apply when the boundary layer is laminar are given in reference (1). The expressions which will be used when the boundary layer is turbulent are taken from the flat plate results given in reference (5) and discussed briefly below.

The flat plate analysis is based on von Kármán's similarity theory for incompressible flow. An apparent Prandtl number near unity is assumed so that the density can be approximated by

$$\frac{\rho_w}{\rho} = \frac{T}{T_w} = 1 + \left(\frac{T_{T_1}}{T_w} - 1\right)\left(\frac{u}{u_1}\right) - \beta\frac{T_{T_1}}{T_w}\left(\frac{u}{u_1}\right)^2 \qquad (2)$$

where

$$\beta = \left(\frac{\gamma-1}{2}M_1^2\right)\Big/\left(1 + \frac{\gamma-1}{2}M_1^2\right) = \left(\frac{T_{T_1}}{T_1} - 1\right)\Big/\left(\frac{T_{T_1}}{T_1}\right)$$

Using equation (2) and taking a constant wall temperature along the plate, a derivation similar to the insulated plate derivation of reference (6) was carried out to obtain the skin friction relations.

$$(\sin^{-1}\eta_l - \sin^{-1}\eta_f)\,(\beta c_f T_{T_1}/T_1)^{-\frac{1}{2}} = -6.43 + \log_{10}\left(\frac{1.6}{S}\,\frac{\mu_1}{\mu_w}\,c_f R\right) \qquad (3)$$

$$0.242\,(\sin^{-1}\eta - \sin^{-1}\eta_F)\,(\beta c_F T_{T_1}/T_1)^{-\frac{1}{2}} = -1.968 + \log_{10}\left(\frac{11.5}{S}\,\frac{\mu_1}{\mu_w}\,c_F R\right) \qquad (4)$$

Taking z here as the distance from the plate leading edge, D as the plate drag, and u_ℓ as the velocity at the edge of the laminar sublayer

$R = \rho_1 u_1 z/\mu_1$

$c_f = 2\tau_w/\rho_1 u_1^2$ = local skin friction coefficient

$c_F = 2D/\rho_1 u_1^2 z$ = mean skin friction coefficient

$S = u_\ell(\tau_w/\rho_w)^{\frac{1}{2}}$

Experimental values of the sublayer parameter, S, have been collected in reference (7) where it is shown that a good fit to the data is given by

$$S = 11.5 + 6.6\,(T_{e_1} - T_w)/T_{e_1} \qquad (5)$$

The recovery temperature, T_{e_1}, for the turbulent boundary layer is given by

$$T_{e_1} = \left(1 + Pr^{\frac{1}{3}}\,\frac{\gamma - 1}{2}\,M_1^2\right) T_1 \qquad (6)$$

The functions η, η_f, and η_F are defined by

$$\eta = \left\{2\beta - (T_{T_1} - T_w)/T_{T_1}\right\}/\Phi$$

$$\eta_f = \left\{2\beta S\left(\frac{T_w}{T_1}\,\frac{c_f}{2}\right)^{\frac{1}{2}} - (T_{T_1} - T_w)/T_{T_1}\right\}/\Phi$$

$$\eta_F = \left\{2\beta S\left(\frac{T_w}{T_1}\,\frac{c_F}{2}\right)^{\frac{1}{2}} - (T_{T_1} - T_w)/T_{T_1}\right\}/\Phi$$

where

$$\Phi = \left\{4\,\beta\left[1 - (T_{T_1} - T_w)/T_{T_1}\right] + \left[(T_{T_1} - T_w)/T_{T_1}\right]^2\right\}^{\frac{1}{2}}$$

Theoretical results based on von Kármán's similarity theory are given in both references (7) and (8). The relations given in both references differ somewhat from equations (3) and (4). The present results have been compared with experimental skin friction coefficients of references (6), (9), (10), (11), (12), and (13) which cover the range of M_1 from 1.7 to 7.0 and $(T_{T_1} - T_w)/T_{T_1}$ from 0.04 to 0.84. There is reasonable agreement between theory and experiment. It should be noted that equations (3) and (4) and the expressions for η, η_f, η_F, and Φ differ slightly from those given in AGARDograph 97. Where the total temperature T_{T_1} appears here, the recovery temperature T_{e_1} appears in AGARDograph 97. The change was made after comparing the analytical results with high Mach number friction drag data recently obtained at the Naval Ordnance Laboratory. With the assumption Pr = 1, it is in fact T_{T_1} which appears in the analysis. The previous use of T_{e_1} was an attempt to account for the fact that $Pr \neq 1$.

To integrate equation (1) over a cone, it is necessary to obtain c_f as a function of R_{θ_1}. It is assumed that the expression derived below for a flat plate applies here. For a flat plate

$$c_F = 2\theta/z = 2R_{\theta_1}/R \tag{7}$$

$$c_f = d(c_F R)/dR \tag{8}$$

With equations (4), (7), and (8) it can be shown that

$$c_f = c_F\left[\frac{-1.968 + \log_{10}\left(\frac{23}{S}\,\frac{\mu_1}{\mu_w}\,R_{\theta_1}\right) + 0.242\left(2\,\beta\,\frac{T_w}{T_{T_1}}\right)^{\frac{1}{2}}\Big/\Phi\left(1-\eta_F^2\right)^{\frac{1}{2}}}{-1.099 + \log_{10}\left(\frac{23}{S}\,\frac{\mu_1}{\mu_w}\,R_{\theta_1}\right) + 0.242\left(2\,\beta\,\frac{T_w}{T_{T_1}}\right)^{\frac{1}{2}}\Big/\Phi\left(1-\eta_F^2\right)^{\frac{1}{2}}}\right] \tag{9}$$

With equation (7), equation (4) can be written

$$0.242\left(\sin^{-1}\eta - \sin^{-1}\eta_F\right)\left(\beta c_F\,\frac{T_{T_1}}{T_1}\right)^{-\frac{1}{2}} = -1.968 + \log_{10}\left(\frac{23}{S}\,\frac{\mu_1}{\mu_w}\,R_{\theta_1}\right) \tag{10}$$

In effect, c_F can now be eliminated between equations (9) and (10). Since this can only be done numerically, equations (9) and (10) serve as

the relation between c_f and R_{θ_1}. The coefficient c_F is merely a parameter which is eliminated numerically when making computations.

The parameters δ/θ and $H = \delta^*/\theta$ have been approximated by assuming that the boundary-layer velocity distribution is given by

$$\frac{u}{u_1} = \left(\frac{y}{\delta}\right)^{\frac{1}{n}} \tag{11}$$

Values of δ/θ and H have been calculated using equations (2) and (11) and the definitions for δ^* and θ. The results can be approximated by

$$\frac{\delta}{\theta} = \frac{(n+1)(n+2)}{n + 2\,(T_{T_1} - T_W)/T_{T_1}} + \frac{\gamma - 1}{2} M_1^2 \left\{1.34 + 1.38 \left(1 - \frac{T_{T_1} - T_W}{T_{T_1}}\right)\right\} \tag{12}$$

$$H = \frac{n+2}{n}\left(1 - \frac{T_{T_1} - T_W}{T_{T_1}}\right) + \frac{\gamma - 1}{2} M_1^2 \left\{1 + 1.20 \left(1 - \frac{T_{T_1} - T_W}{T_{T_1}}\right)\right\} \tag{13}$$

Values of δ/θ and H are not very sensitive to n which, from experiment, varies slowly with Reynolds number. For a nominal value of $n = 7$, a range of M_1^2 from 0 to 95 and $\left(T_{T_1} - T_W\right) / T_{T_1}$ from 0 to 1, the agreement between the numerical results and equations (12) and (13) is generally better than 3% and 1.5%, respectively.

The derivative $d\left[(\delta/\theta) - H\right]/dM_1$ will be required later. For T_W = constant and n = constant, the following result can be obtained from equations (12) and (13)

$$\frac{d\left[(\delta/\theta) - H\right]}{dM_1} = (\gamma - 1) M_1 \left[0.34 + 0.18 \left(\frac{T_{T_1} - T_W}{T_{T_1}}\right)\right] \tag{14}$$

Mach Number Gradient

Reference (1) presents two relations between the local Mach number, M_1, at the outer edge of the boundary layer and the local shock wave angle, ω_S. The first relation is derived by equating the mass flow in the boundary layer to that in a stream tube ahead of the bow shock. The bow shock is assumed to be hyperbolic and described by

$$a^2/r_S^2 = \tan^2 \omega_S - \tan^2 \omega \tag{15}$$

where the shock curvature on the axis, a, is related to the body nose

radius by a ≈ 1.5b. The relation is

$$\frac{P_\infty M_\infty}{P_1 M_1}\left(\frac{2+(\gamma-1)M_\infty^2}{2+(\gamma-1)M_1^2}\right)^{\frac{1}{2}}\left(\frac{a^2}{\tan^2\omega_S-\tan^2\omega}\right)=2r\theta\left(\frac{\delta}{\theta}-H\right) \tag{16}$$

The second relation assumes isentropic flow along each streamline from the bow shock to the outer edge of the boundary layer. With this assumption and the oblique shock equations for a perfect gas

$$\left(1+\frac{\gamma-1}{2}M_1^2\right)\left(\frac{P_1}{P_\infty}\right)^{\frac{\gamma-1}{\gamma}}=\frac{(\gamma+1)M_\infty^2\sin^2\omega_S\left[2+(\gamma-1)M_\infty^2\right]}{2\left[2+(\gamma-1)M_\infty^2\sin^2\omega_S\right]}\left[\frac{\gamma+1}{2\gamma M_\infty^2\sin^2\omega_S-(\gamma-1)}\right]^{\frac{1}{\gamma}} \tag{17}$$

Making use of the assumption that P_1 = constant on the cone, differentiating equations (16) and (17) with respect to x and eliminating $d\omega_S/dx$ results in an expression which can be used for calculating the Mach number gradient, dM_1/dx.

$$\frac{2\theta}{M_1\left[2+(\gamma-1)M_1^2\right]}\left\{\frac{2+(\gamma-1)M_1^2-\left[(\delta/\theta)-H\right]}{F_1}\right\}\frac{dM_1}{dx}=\frac{d\theta}{dx}+\frac{\theta}{r}\frac{dr}{dx} \tag{18}$$

where

$$F_1=-\left\{2+(\gamma-1)M_1^2-\left(\frac{\delta}{\theta}-H\right)\right\}\Big/\left\{1+(\gamma-1)M_1^2+\frac{M_1\left[2+(\gamma-1)M_1^2\right]}{2\left[(\delta/\theta)-H\right]}\frac{d\left[(\delta/\theta)-H\right]}{dM_1}-\right. \tag{19}$$

$$\left.\frac{M_1^2\tan^2\omega_S\sec^2\omega_S\left[2\gamma M_\infty^2\sin^2\omega_S-(\gamma-1)\right]\left[2+(\gamma-1)M_\infty^2\sin^2\omega_S\right]}{2\left(\tan^2\omega_S-\tan^2\omega\right)\left(M_\infty^2\sin^2\omega_S-1\right)^2}\right\}$$

For the laminar boundary layer case treated in reference (1), the difference (δ/θ) - H which appears in equations (16), (18), and (19) above (and also in equation (1)) is constant. For the turbulent case this is not true and complicates the calculations. Equations (12) and (13) must be used to calculate (δ/θ) - H and equation (14) must be used to calculate $d\left[(\delta/\theta)-H\right]/dM_1$ which appears in equation (19).

Integration of the Momentum Equation

Making use of the definitions for $R_{\theta c}$ and R_{xc}, equations (1) and (18) yield

$$\frac{dR_{\theta c}}{dR_{xc}} = \frac{c_f}{2}\left(\frac{1}{1+F_1}\right) - \frac{R_{\theta c}}{R_{xc}} \tag{20}$$

Integration of equation (20) for the laminar case is treated in reference (1). For the turbulent case, the integration starts at the transition point where $R_{xc} = R_{xctr}$ and $R_{\theta c} = R_{\theta ctr}$. The integral form of equation (20) is then

$$R_{\theta c} = R_{\theta ctr} + \int_{R_{xctr}}^{R_{xc}} \left\{\frac{c_f}{2}\left(\frac{1}{1+F_1}\right) - \frac{R_{\theta c}}{R_{xc}}\right\} dR_{xc} \tag{21}$$

In order to obtain $R_{\theta c}$ as a function of R_{xc} from equation (21), the value of eitner $R_{\theta ctr}$ or R_{xctr} must be known or assumed. The other value is obtained by integrating equation (20) for the laminar portion of the boundary layer using reference (1). To proceed with the integration, equation (21) is used with c_f given by equations (9) and (10) and F_1 given by equation (19). It should be noted that to obtain c_f as a function of $R_{\theta c}$, put $R_{\theta 1} = \rho_1 u_1 \mu_c R_{\theta c}/\rho_c u_c \mu_1$ in equations (9) and (10). With constant pressure on the cone and adiabatic flow outside the boundary layer, $\rho_c u_c/\rho_1 u_1 = M_c T_1^{\frac{1}{2}}/M_1 T_c^{\frac{1}{2}}$ and $T_1/T_c = [2 + (\gamma-1)M_c^2]/[2 + (\gamma-1)M_1^2]$. As equation (21) is integrated, the value of M_1 is obtained along the cone by finding the values of M_1 and ω_s at each point which satisfy equations (17) and (16) which may be written

$$\frac{R_{xc}R_{\theta c}}{R_{bc}^2} = \frac{\dfrac{1.125}{\sin\sigma}\dfrac{P_\infty M_\infty}{P_1 M_1}\left[\dfrac{2+(\gamma-1)M_\infty^2}{2+(\gamma-1)M_1^2}\right]^{\frac{1}{2}}}{\left[(\delta/\theta)-H\right](\tan^2\omega_s - \tan^2\omega)} \tag{22}$$

The above method assumes that θ is continuous at the transition point. This results in discontinuities in the other thicknesses, δ^* and δ. In addition, there is a discontinuity in M_1 corresponding to the discontinuity in δ. This results from the Mach number gradient normal to the surface caused by the shock curvature. The value of M_1 for the

turbulent boundary layer at the transition point can be obtained from equations (17) and (22). Put the transition point values of R_{xc} and $R_{\theta c}$ in equation (22) and calculate the value of (δ/θ) - H required from equations (12) and (13).

As equation (21) is integrated to obtain $R_{\theta c}$ and local properties along the cone, the local skin friction is determined at each point and all the thicknesses (θ, δ^*, and δ) can be calculated. As in reference (1), the heat-transfer rate can be calculated assuming that the Stanton number is given by the flat plate Reynolds analogy. For the turbulent boundary layer the local recovery temperature must be determined for each point from equation (6).

It should be noted that equation (21) applies to the case of a sharp cone by putting $F_1 = 0$.

Numerical and Experimental Results

Figure 2 presents numerical results showing the variation of local Mach number along an 8° half angle cone with three bluntnesses. The flow passing through the curved portion of the bow shock forms a variable entropy layer over the cone. As the boundary layer swallows this variable entropy layer, the local Mach number increases and approaches the sharp cone value. The solid curves, taken from reference (1), show the effect of nose radius Reynolds number, R_{bc}, on the laminar boundary layer. Experimental results discussed later indicate that the momentum thickness Reynolds number based on local properties, R_{θ_1}, may be approximately 800 at transition. Assuming no dependence on Mach number and taking this value, the dotted curves on figure 2 show the great effect of the turbulent boundary layer on local Mach number. For the lowest value of R_{bc}, the sharp cone Mach number is reached before transition occurs. The aft movement of transition with increasing R_{bc} is due to the decreasing local unit Reynolds number and the assumption that R_{θ_1} at transition is constant.

References (2) and (3) give a method for calculating the local Mach number variation for the laminar boundary layer. Instead of integrating the momentum equation as is done here, the method assumes local boundary layer similarity and makes use of a mass flow function given by reference (4). The momentum-integral results from reference (1) are compared on figure 3 with results using references (2) and (3). The bow shock given by equation (15) was used for all calculations. There is a great difference between the results of references (1) and (2).

References (1) and (3) are in good agreement for the case calculated. In reference (2) the ratio of local stagnation pressure to Pitot pressure was included in defining a transformed coordinate along the body. There seemed no justification for including this ratio and it was omitted when the same authors prepared reference (3).

The effect of a slight bluntness on local conditions can significantly affect the interpretation of experimental data. The interpretation of transition data from ballistics range firings is a pertinent example. Figure 4 taken from reference (14) presents drag coefficient data for a slightly-blunted cone. As the freestream Reynolds number is increased, transition moves upstream in the wake. At some Reynolds number the wake will be completely turbulent and transition will be located at the base of the body. With a further increase in Reynolds number, transition moves forward on the body and the drag rises. The open symbols on figure 4 indicate that the base flow was laminar on shadow photographs. The solid symbols indicate that the base flow was completely turbulent. At the freestream Reynolds number for which the drag rise begins, transition occurs at the base. The drag curve can thus be used to determine a transition Reynolds number for slender cones. This is a useful technique at hypersonic speeds when the shock is so close to the surface that the boundary layer is difficult to see on a schlieren or shadow photograph. When the cone is slightly blunted, a difficulty now arises in stating the local Mach number and Reynolds number at which transition occurs. In order to resolve this difficulty, the boundary-layer growth over the body must be calculated. Laminar flow only need be considered since transition occurs at the base. Values of R_{bc} at transition of 3.8×10^4 and 6.3×10^4 were computed at Mach numbers of 9 and 13.3, respectively, for the data shown on figure 4. For these values of R_{bc}, the boundary layer growth over the cone was computed using the method of reference (1). The variations in Mach number over the cone are shown on figure 5. The arrows marked transition indicated the values of R_{xc} at the base of the cone. It is evident that the swallowing process had not been completed at either Mach number 9 or 13.3 when transition occurred. Using the boundary-layer calculations, the actual transition conditions can be compared with those which would be obtained if the bluntness were neglected and the cone assumed to be sharp. Figure 6 shows the transition Reynolds number based on length along the cone as a function of Mach number. In one case the Reynolds number is based on local conditions at the base and the local Mach number is plotted on the abscissa. This is compared with the base where Reynolds number based on sharp cone conditions is plotted vs. the sharp cone Mach number. The magnitudes of the results are quite different and, in addition, the trend of transition Reynolds number with Mach number

is different. It is perhaps more pertinent to plot values of R_θ vs. M at transition for the blunt and sharp cone. These data are shown on figure 7 and the comment made for figure 6 can be repeated. At a Mach number of 7, the data indicate that the local Reynolds number, R_{θ_1}, at transition is about 800.

Slight blunting can significantly affect the local shear stress. Calculations for the laminar boundary layer taken from reference (1) are shown on figure 8. The ratio $c_{f_c}/c^0_{f_c}$ is equal to the ratio of the wall shear stress on the blunted cone to that on a sharp cone, since both skin friction coefficients are based on the sharp cone dynamic pressure. The results of figure 8 show that the bluntness should be taken into account when calculating the friction drag. Reference (14) presents experimental and calculated values of total drag coefficient for fully laminar cones. The data are plotted in reference (14) vs. the hypersonic interaction parameter. They are replotted here on figure 9 as a function of free-stream Reynolds number. There is good agreement between calculation and experiment. The calculations included the pressure drag on the cone, the base drag, the friction drag calculated using the method of reference (1), an induced pressure correction to the cone pressure drag, and induced pressure and transverse curvature corrections to the friction drag. However, the difference between the cone pressure drag coefficient shown on figure 9 and the total drag coefficient is largely due to the friction drag calculated using the method of reference (1). This indicates that the momentum-integral method for slightly-blunted cones gives reliable laminar friction drag predictions. It is of interest to note from figure 9 that, when plotted vs. freestream Reynolds number, the total drag coefficient seems to be almost independent of Mach number.

In deriving the momentum-integral equation, equation (1), it was assumed that the shear stress at the outer edge of the boundary layer could be neglected; i.e., $2\tau_1/\rho_1 u_1^2 \ll c_f$. Reference (1) stated that this assumption had been checked for the numerical results given on figure 8. This check can be made as follows. The change in u_1 in the y direction between two adjacent streamtubes at the outer edge of the boundary layer is equal to the change in u_1 in the x direction between the two points at which these streamtubes enter the boundary layer. In addition, the mass flow between these two streamtubes is equal to the increase in the mass flow in the boundary layer. From these statements it follows that

$$\left(\frac{\partial u}{\partial y}\right)_1 = \rho_1 u_1 r \frac{du_1}{dx} \Big/ \frac{d}{dx}\left(r\int_0^\delta \rho u dy\right)$$

The value of τ_1 is given by

$$\tau_1 = \mu_1 \left(\frac{\partial u}{\partial y}\right)_1$$

With the above relations and equations (18) and (20), it can be shown for the case of laminar flow on a cone, where $(\delta/\theta) - H = \text{constant} = 6.41$, that

$$\frac{2\tau_1/\rho_1 u_1^2}{c_f} = \frac{\tau_1}{\tau_w} = \left\{3.405\, c_f R_{\theta_1}\left[1 + (\gamma-1)M_1^2\right] + \frac{(\gamma-1)M_1^2 - 4.41}{F_1}\right\}^{-1}$$

The above result is independent of the bluntness Reynolds number, R_{bc}.

Making use of reference (1) to compute $c_f R_{\theta_1}$ and F_1, τ_1/τ_w has been computed and plotted vs. M_1 on figure 10. This result applies to all three bluntnesses on figure 8. It can be seen that the error in neglecting τ_1 is small.

Figure 11 shows a shadow photograph from a ballistics range shot of a 9° half angle cone at a freestream Mach number of 10.3. The enlargement shows the flow in the base region. The boundary layer is almost completely turbulent and data which can be obtained from the shot have been compared with calculations. The boundary-layer growth was calculated using reference (1) for the laminar region and the present results for the turbulent region. A value of $n = 7$ was used for the velocity distribution of equation (11). Although the location of transition is impossible to determine accurately, it appeared from an enlargement of figure 11 to occur about 20% of the body length from the nose. On integrating the momentum-integral equation, it was found that R_{θ_1} at transition was approximately 300. The computed variation in Mach number at the outer edge of the boundary layer is shown on figure 12. It can be seen that transition occured at $M_1 \approx 3$. The value of R_{θ_1} in this case is much less than the value of 800 at $M_1 \approx 7$ given on figure 7. It should be noted that there was appreciable melting of the tip of the model shown on figure 11. This was not the case for the data of figure 4. The computed variation of boundary-layer thickness, δ, is shown on figure 13. Values of δ at the base were measured at the top and bottom of the body from an enlargement of figure 11. Measurements were also made on a repeat shot. The agreement between calculation and experiment on figure 13 is remarkable and probably fortuitous considering the difficulty in defining the edge of the boundary layer. Total drag measurements were made for the two shots. The measured drag coefficients of 0.0854 and 0.0839 compare with a calculated value of 0.0929. The check between calculation and experiment is reasonable. However, no statement can be

made about agreement between experiment and calculated friction drag. This is due to uncertainties in base pressure and model tip diameter and the fact that the friction drag was only about 20% of the total. At this point it is of interest to return to figure 4, where the check between calculated and experimental drag results is quite good. At the higher Reynolds numbers when considerable turbulent flow exists, the friction drag is 30% or more of the total. This increase in the relative magnitude of the friction drag is due primarily to the small cone half angle of 6.3°. The friction drag when turbulent flow was present was calculated for figure 4 assuming a constant R_{θ_1} at transition.

One of the interesting features of figure 11 is the very wide turbulent wake in the base region, with the trailing shocks originating deep inside the wake. From the calculations of boundary-layer thickness and also from figure 11, it is apparent that the boundary layer occupies about half of the region between the model surface and the bow shock. Thus when the flow expands around the corner at the base, a great part of the base region is filled with the boundary-layer flow.

REFERENCES

1. Wilson, R. E., "Laminar Boundary-Layer Growth on Slightly-Blunted Cones at Hypersonic Speeds," J. Space. Rockets 2, pp 490-496, 1965

2. Zakkay, Victor and Krause, Egon, "Boundary Conditions at the Outer Edge of the Boundary Layer on Blunted Conical Bodies," Aero. Res. Labs, p 62-386, 1962

3. Zakkay, Victor and Krause, Egon, "Boundary Conditions at the Outer Edge of the Boundary Layer on Blunted Conical Bodies," AIAA Jour. Vol. 1, No. 7, pp 1671-1672, 1963

4. Lees, L., "Laminar Heat Transfer Over Blunt-Nosed Bodies at Hypersonic Flight Speeds," Jet Propuls. Vol. 26, pp 259-269, 1956

5. Wilson, R. E., "The Hypersonic Turbulent Boundary Layer With Heat Transfer," NOLTR 65-91, 1965

6. Wilson, R. E., "Turbulent Boundary-Layer Characteristics at Supersonic Speeds--Theory and Experiment," J. Aero. Sci., Vol. 17 No. 9, 1950

7. Harkness, John L., "The Effect of Heat Transfer on Turbulent Boundary Layer Skin Friction," DRL-436, CM-940, 1959

8. Van Driest, E. R., "Turbulent Boundary Layer With Variable Prandtl Number," No. Amer. Avia., Inc. Rpt AL-1914, 1954

9. Coles, Donald, "Measurements in the Boundary Layer on a Smooth Flat Plate in Supersonic Flow. III. Measurements in a Flat-Plate Boundary Layer at the Jet Propulsion Laboratory," JPL Rpt 20-71, 1953

10. Korkegi, R. H., "Transition Studies and Skin Friction Measurements on an Insulated Flat Plate at a Mach Number of 5.8," J. Aero. Sci., Vol. 23, No. 2, p. 97, 1956

11. Matting, F. W., et al, "Turbulent Skin Friction at High Mach Numbers and Reynolds Numbers in Air and Helium," NASA TR R-82, 1961

12. Winkler, E. M. and Cha, M. H., "Investigation of Flat Plate Hypersonic Turbulent Boundary Layers With Heat Transfer at a Mach Number of 5.2," NOL NavOrd Rpt 6631, 1959

13. Sommer, S. C. and Short, B. J., "Free-Flight Measurements of Turbulent-Boundary-Layer Skin Friction in the Presence of Severe Aerodynamic Heating at Mach Numbers from 2.8 to 7.0," NACA TN 3391, 1955

14. Sheetz, N., "Free-Flight Boundary-Layer Transition at Hypersonic Speeds," presented at AIAA mtg, New York, Jan 1965

15. Lyons, W. C., Jr., Brady, J. J., and Levensteins, Z. J., "Hypersonic Drag, Stability, and Wake Data for Cones and Spheres," AIAA Jour., Vol. 2, No. 11, 1964

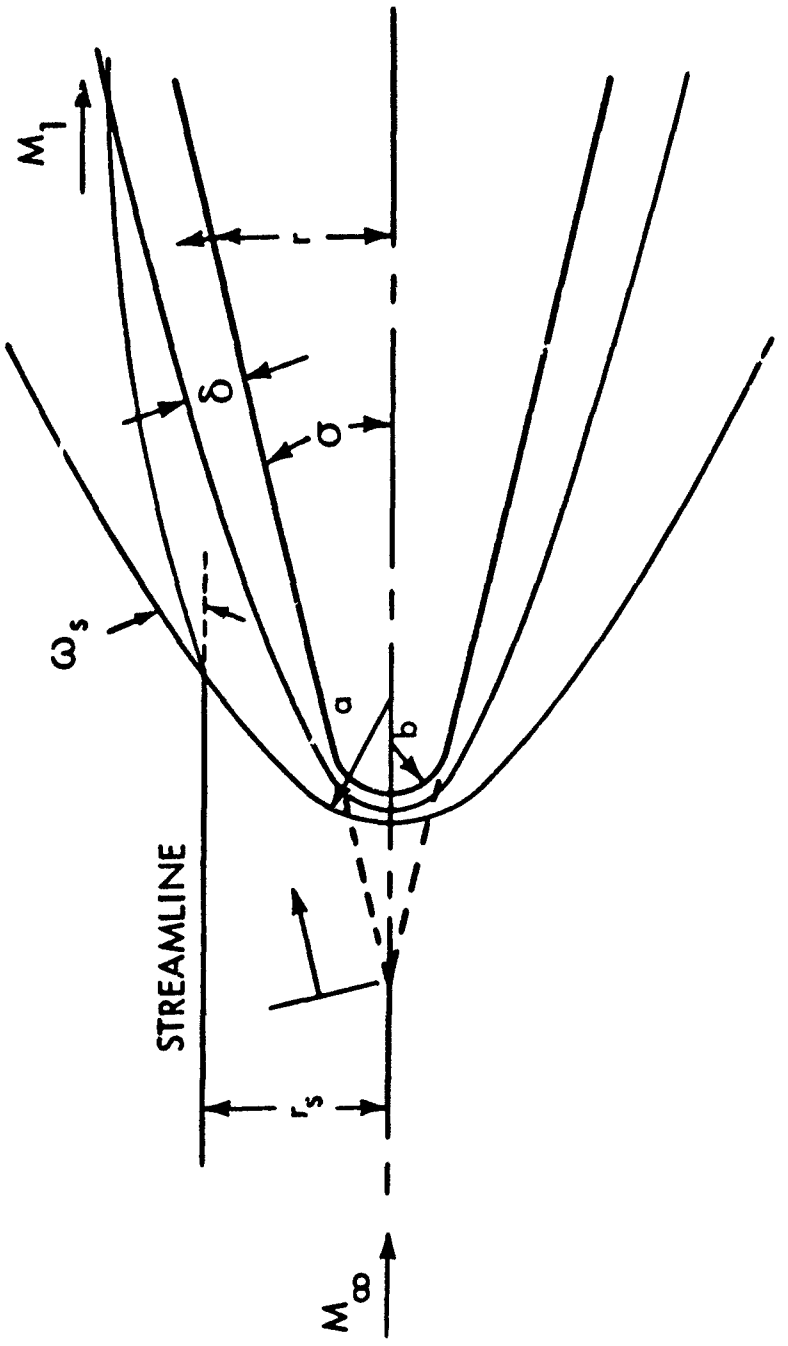

FIG. 1 COORDINATE SYSTEM

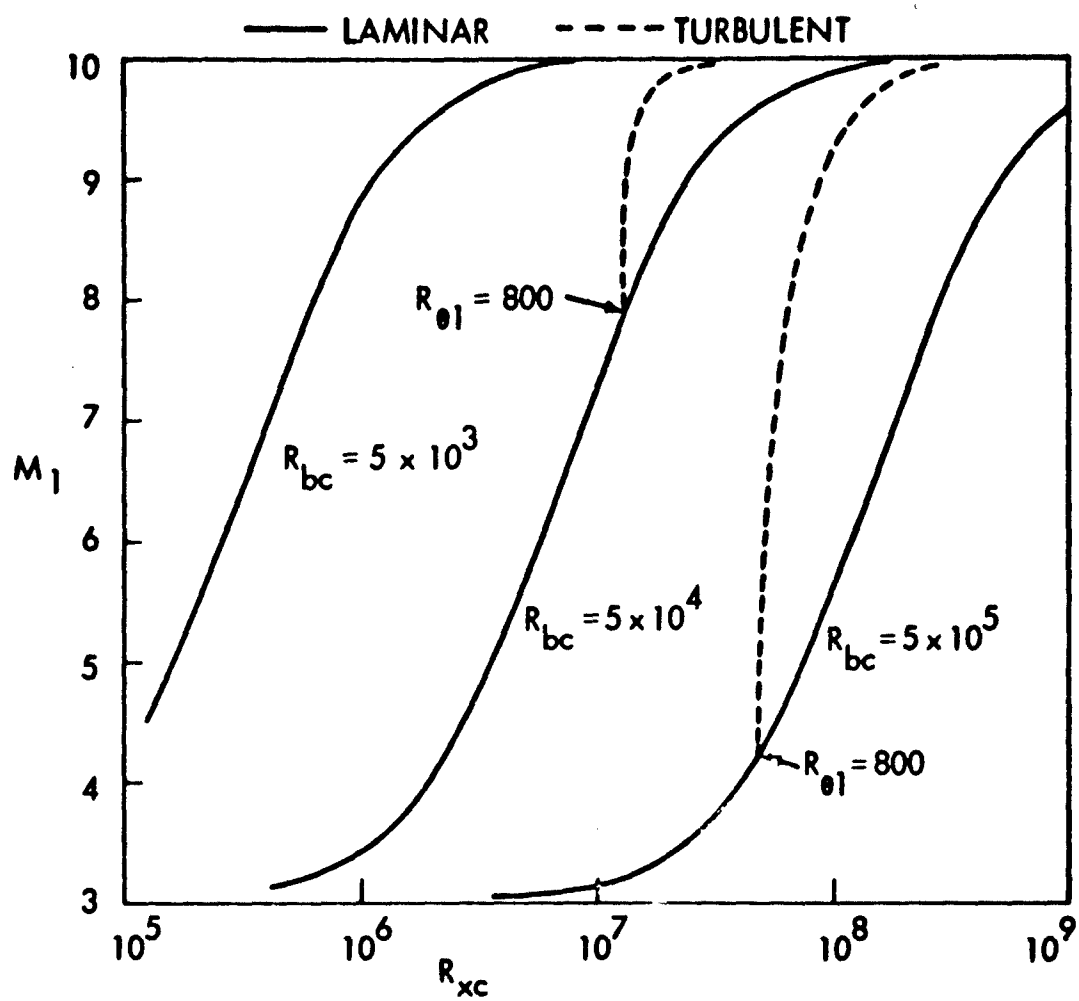

FIG. 2

EFFECT OF BLUNTNESS ON LOCAL MACH NUMBER
$M_\infty = 14.9$, $M_c = 10.0$, $\sigma = 8°$, $T_\infty = T_w = 530°R$

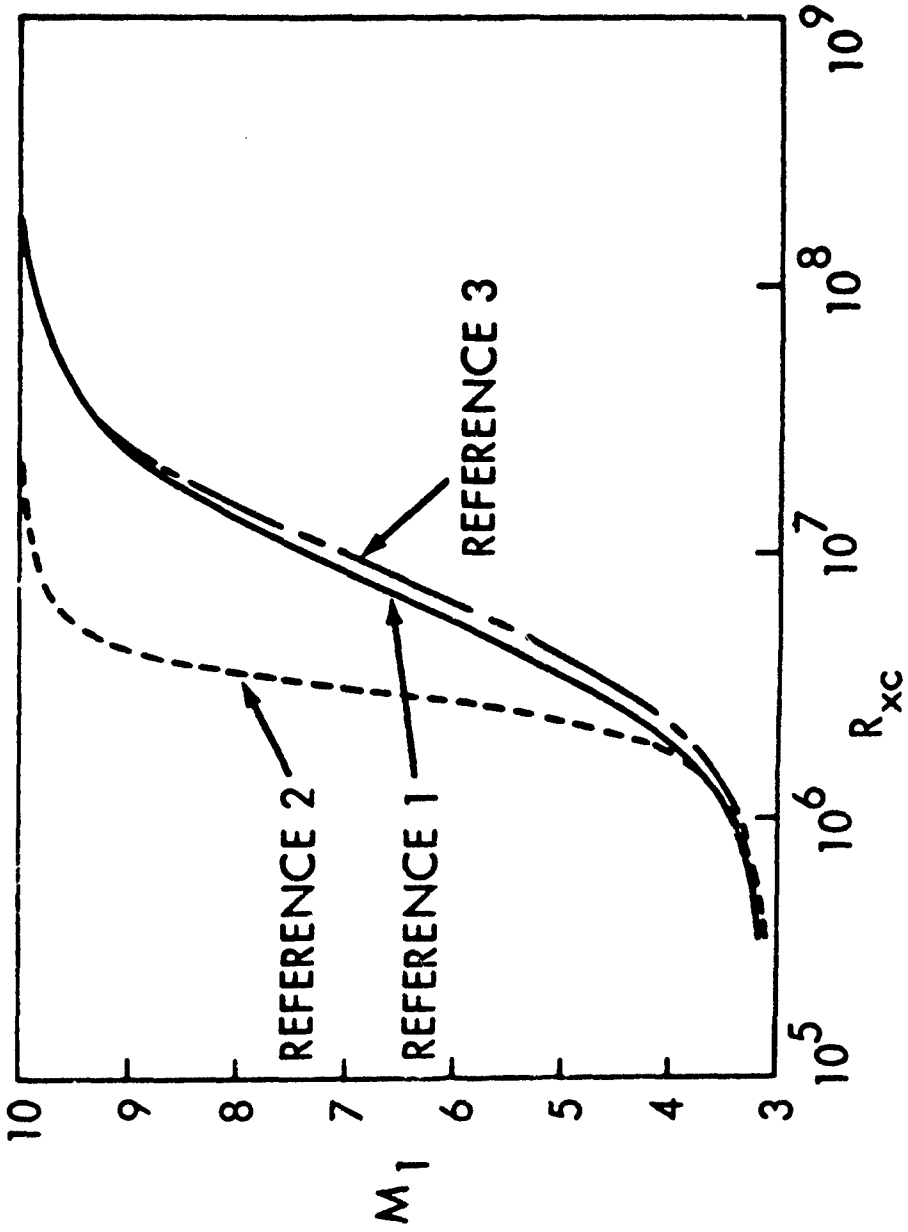

FIG. 3

COMPARISON OF METHODS: $M_\infty = 14.9$, $M_c = 10.0$

$\sigma = 8°$, $T_\infty = T_w = 530°R$, $R_{bc} = 5.0 \times 10^4$

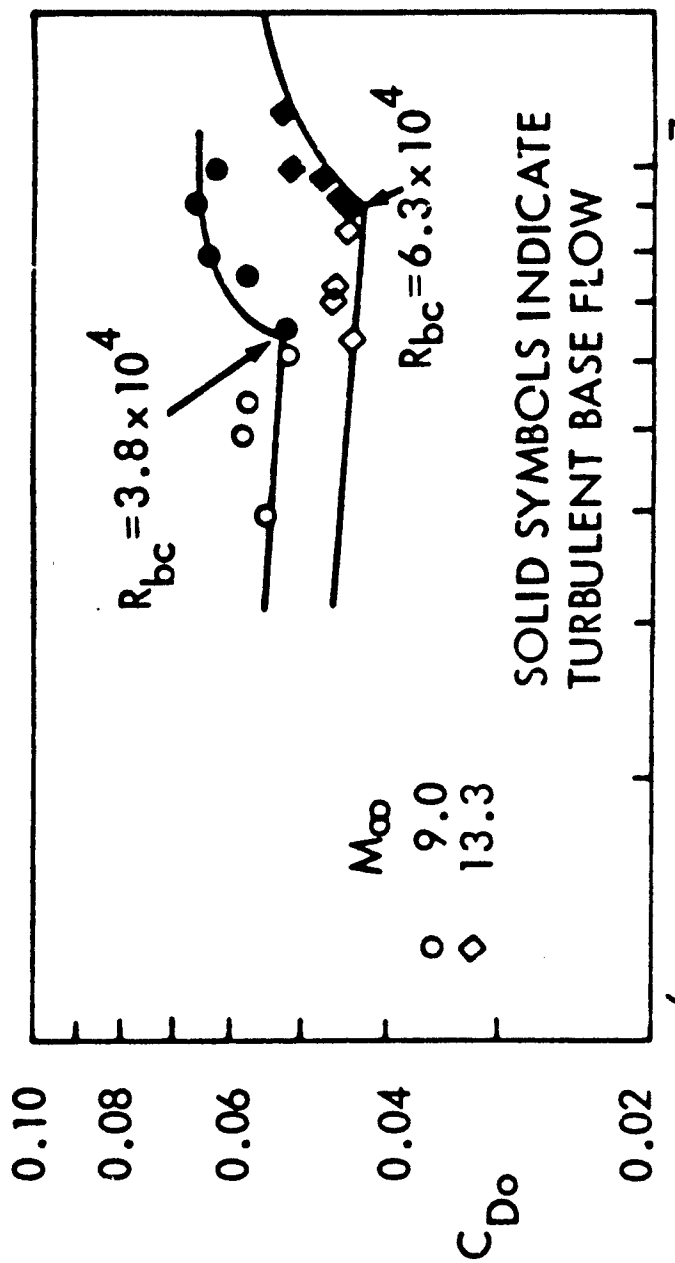

FIG. 4

COMPARISON OF CALCULATED AND EXPERIMENTAL CONE DRAG COEFFICIENTS: $\sigma=6.3°$, $b/B=0.035$, $T_\infty=T_w=540°R$